Combined GPS+BDS+Galileo+QZSS for Long Baseline RTK Positioning

R. Odolinski[1], P.J.G Teunissen[1,2], D. Odijk[1]
1) *GNSS Research Centre, Department of Spatial Sciences*
Curtin University, Perth, Australia
2) *Mathematical Geodesy and Positioning*
Delft University of Technology, The Netherlands

BIOGRAPHY

Robert Odolinski received in 2009 his MSc degree in Geodesy at the Royal Institute of Technology (KTH), Stockholm, Sweden. In 2011 he started his PhD studies at Curtin University, Australia. His research topic is next generation multi-GNSS integer ambiguity resolution enabled precise positioning.

Peter J.G. Teunissen is a Federation Fellow of the Australian Research Council (ARC), Professor of Geodesy and Navigation and Head of Curtin's GNSS Research Centre. His current research focus is on modeling next-generation GNSS for improved parameter estimation and validation.

Dennis Odijk is a Research Fellow in the GNSS Research Centre at Curtin University. His research is focused on high-precision GNSS positioning, with an emphasis on integer ambiguity resolution enabled precise point positioning, ionospheric modeling, multi-GNSS interoperability, quality control and prototype software development.

ABSTRACT

In this contribution we will focus on long single-baseline real-time kinematic (RTK) positioning when combining the American GPS, Chinese BDS, European Galileo and Japanese QZSS. The main objective is to demonstrate the potential benefits for RTK when combining the next generation GNSSs, as compared to using the systems separately. With long baseline we refer to the necessity to model the slant ionospheric delays by the ionosphere-float strategy. The (wet) Zenith Tropospheric Delay (ZTD) will be estimated as well. The ionosphere-float model implies that the slant ionospheric delays are assumed completely unknown. We will focus on overlapping frequencies between the systems. The advantage with overlapping frequencies is that the redundancy of the model can be maximized if the inter-system biases (ISBs) can be calibrated. This also allows for a common pivot satellite between the systems when parameterizing the double-differenced integer ambiguities. It will be shown that with the ionosphere-float model at least two overlapping frequencies between the systems are required to benefit from calibration of ISBs. The GNSS real data is collected in Perth Australia, a country where the multi-system satellite visibility is almost at a global maximum. The single-baseline RTK performance is evaluated by a formal and empirical analysis, consisting of ambiguity dilution of precision (ADOP), bootstrapped success rates and positioning precisions. It will be shown that the combination of the four systems provides for shorter ambiguity/positioning convergence times, improved integer ambiguity resolution and positioning performance over the single-, dual- and triple-systems.

INTRODUCTION

Precise positioning applications using the next generation Global Navigation Satellite Systems (GNSSs) have the potential to improve, provided that a combination of the systems is used. This since already today (2014) we have 32 American Global Positioning System (GPS), 14 Chinese BeiDou Navigation Satellite System (BDS), 4 European Galileo, and 1 Quasi-Zenith Satellite System (QZSS) satellites available for positioning. In addition the Russian GLONASS is available with around 24 satellites [1]. But in contrary to the other Code Division Multiple Access (CDMA) systems, the majority part of the GLONASS satellites are based on the Frequency Division Multiple Access (FDMA) and will thus not be used in this contribution.

The 32 GPS satellites transmit on the L1, L2 frequencies, and currently six satellites also on the modernized L5 frequency (Table 1). BDS is an Asia-Pacific regional

constellation, but will by 2020 become global and consist of 5 Geostationary Earth Orbit (GEO), 3 Inclined Geo-Synchronous Orbit (IGSO) and 27 Medium Earth Orbit (MEO) satellites [2]. BDS broadcasts signals on the B1, B2 and B3 frequencies (Table 1). Since 2005 and 2008, respectively, two Galileo In-Orbit Validation Element (GIOVE) satellites have been in orbit, but they are currently not available for positioning. However at this moment (2014) four Galileo In-Orbit Validation (IOV) MEO satellites are available (since 2012) for positioning [3], which broadcast signals at the E1, E5a, E5b and E6 frequencies (Table 1). The E6 frequency will only be received as part of Galileos commercial service. Galileo is intended to be a global constellation once it reaches its full constellation by 2020, with 27 MEO and 3 spare satellites. The QZSS is to be developed as an Asia-Pacific regional constellation. QZSS uses the same orbital period as a traditional equatorial geostationary orbit and a large orbital inclination, as to enable Japanese users to receive QZSS signals from a high elevation angle at all times. The QZSS broadcasts signals on the L1, L2 and L5 frequencies (Table 1). One Highly-inclined Elliptical Orbit (HEO) satellite 'MICHIBIKI' (or 'QZS-1') is currently in orbit, and was launched in September 2010. By 2018 the QZSS constellation is planned to consist of 3 GEO and 4 HEO satellites [4].

Some first BDS-only results based on real data were presented in, e.g., [5] for BDS single point positioning (SPP) and single-baseline real-time kinematic (RTK) positioning based on an initial BDS constellation of 3 GEO and 3 IGSO satellites. Some first BDS-only RTK positioning results outside of China can be found in [6]. Single-baseline RTK contributions using the current regional BDS constellation that consists of 14 BDS satellites can be found in, e.g., [7–10]. Positioning results for combined GIOVE+GPS single-baseline RTK were presented in [11]. It was shown that the code/phase intersystem biases (ISBs) on the overlapping frequencies between those systems are zero for similar receiver types, but exist for mixed receiver types. The nature and behavior of the GIOVE-GPS ISBs were also investigated in [12], and for IOV-GPS ISBs in [13, 14], which confirmed the results of [11].

Table 1: GPS, BDS, Galileo and QZSS signals

Sat. system	Band	Freq. [MHz]	Wavelength [cm]
BDS	**B1**	1561.098	19.20
BDS/Galileo	**B2**/E5b	1207.140	24.83
BDS	B3	1268.520	23.63
QZSS, GPS/Galileo	**L1/E1**	1575.42	19.03
QZSS, GPS	**L2**	1227.60	24.42
QZSS, GPS/**Galileo**	L5/**E5a**	1176.45	25.48

Table 1 shows the different frequencies available from the

four satellite systems analyzed, and the frequencies used in this contribution are marked in bold. With long single-baseline RTK we refer to the necessity to model the ionospheric and tropospheric delays, here referred to as the ionosphere-float and Zenith Tropospheric Delay (ZTD) float models. As a consequence of having the ionosphere-float model, the number of overlapping frequencies required between the systems, to allow for strengthening of the model when the ISBs are calibrated, are at least *two*. This since the code ISBs are only estimable on the second frequency and beyond. This will be further elaborated on in the description of the single-baseline RTK functional models. Since the GPS L5 frequency is currently (2014) only available from six satellites, we restrict our analysis to the L1, L2 frequencies. That leaves us with two possible overlapping frequencies for GPS with the other systems in Table 1, namely the L1,L2 frequencies of QZSS. In other words, the calibration of ISBs to strengthen the RTK model is herein only possible between QZSS-GPS. In [11, 15], however, it was shown for the ionosphere-fixed case (short baselines) when combining GPS, BDS, Galileo and QZSS, that *one* overlapping frequency between the systems is sufficient to strengthen the RTK model accordingly.

The ground tracks of BDS, Galileo and QZSS as seen from a station in Perth, Australia are depicted in Figure 1. As the signals on the E5a frequency could not be tracked at this time for the E11 satellite, three out of four available Galileo IOV satellites will be used in this contribution.
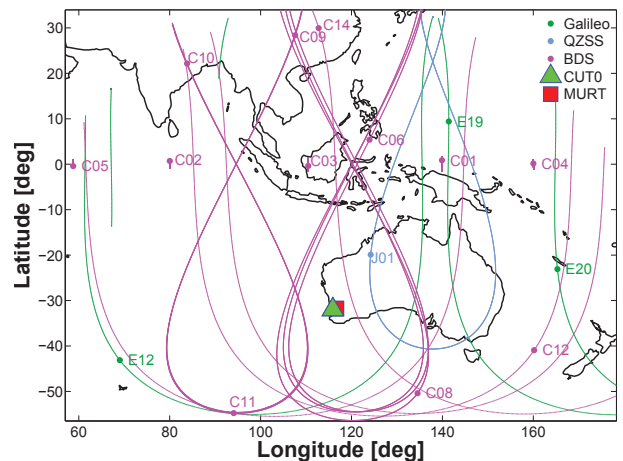

Figure 1: BDS (*magenta*), Galileo (*green*) and QZSS (*cyan*) constellation (February 19, 2014) with satellites location depicted as a *dot* at 15:15 local Perth time for a cut-off angle of 10°. Perth stations CUT0 and MURT are depicted as well

This contribution is organized as follows. First we present the ionosphere-float, ZTD-float single-baseline RTK functional, stochastic and dynamic models used. Two functional models will be given, one referred

to as the "ISBs-float" model where the ISBs are parameterized as unknowns, and one when they are assumed calibrated, the "ISBs-fixed" model. This follows by a description of the GNSS data and the dynamic/stochastic model settings used. A formal analysis of the GPS+BDS+Galileo+QZSS single-baseline RTK performance is then conducted, involving ambiguity dilution of precision (ADOP), bootstrapped success rate, ambiguity convergence times, and the positioning performance. An empirical analysis of the ambiguity/positioning convergence times and positioning performance is then presented based on real data. Emphasis will be on analyzing the combined four-system RTK models, and comparisons will be made to GPS and other possible combinations of the systems. We end this contribution with some conclusions.

SINGLE-BASELINE RTK FUNCTIONAL, STOCHASTIC AND DYNAMIC MODELS

In this Section we will present the ionosphere-float, ZTD-float functional and stochastic models used for the combination of GPS+BDS+Galileo+QZSS. The inter-system biases (ISBs) float and fixed models will be presented, and it will be assumed that all frequencies overlap between the systems for notational convenience. We end the section by describing the redundancy and dynamic model used in the Kalman filter.

ISBs-float, ionosphere-float functional model

In the following observation equations it is assumed that $r = 1, 2$ receivers track, at the same instance, the satellites $s_G = 1_G, \ldots, m_G$ and $s_* = 1_*, \ldots, m_*$ on *overlapping* frequencies $j = 1, \ldots, f$, where m_G, m_*, f is the number of satellites and frequencies respectively. The symbol G is for GPS and $*$ for BDS (B), Galileo (E) or QZSS (Q). The time stamps will be omitted in the equations for brevity, and external products are used for satellite orbits. Since between-receiver single-differences (SDs) are performed on the observation equations, the satellite delays common to both receivers are eliminated. The receiver clock is furthermore shared among the systems, and the time-offsets, e.g., GPS-to-Galileo-time-offset (GGTO), are also eliminated by the SDs. The baseline is assumed to be of a length of at most a few hundred kilometers, thus any remaining satellite orbit errors can be assumed negligible.

The system of observation equations is however not of full-rank after the SDs. The number of rank deficiencies is equal to the number of linear combinations of the column vectors of the design matrix that produces the zero vector. These rank deficiencies can be eliminated through S-system theory [16, 17], which implies null-space identification, S-basis constraining and interpretation of the estimable parameters. The number of rank de-

ficiencies and the S-basis choice for the ionosphere-float and ISBs-float model is given by Table 2. The "ISBs-float" model (1) implies that the ISBs are parameterized as unknowns.

Table 2: Single-epoch single-baseline RTK ionosphere-float, ZTD-float and ISBs-float S-basis choice, and # of rank deficiencies for GPS (G) and $*$ (B for BDS, E for Galileo and Q for QZSS), assuming *overlapping* frequencies between systems

Model	S-basis choice	# of rank defects
Iono-float (ISBs-float)	$\Delta x_1, \tau_1, dt_1,,$ $d_{2,1}^G, d_{2,2}^G, \iota_1^{s_G}, d_{1,j}^G, \delta_{1,j}^G, z_{2,j}^{1_G}, z_{1,j}^{s_G}$ $d_{2,1}^*, \iota_1^{s_*}, d_{1,j}^*, \delta_{1,j}^*, z_{2,j}^{1_*}, z_{1,j}^{s_*}$	$4+1+$ $+2 + m_G + 3f + fm_G +$ $+1 + m_B + 3f + fm_B$ $+1 + m_E + 3f + fm_E$ $+1 + m_Q + 3f + fm_Q$

We have in Table 2 the S-basis consisting of the pivot receiver $r = 1$ coordinates (Δx_1), ZTD (τ_1) and clock (dt_1) that solve for $4 + 1$ rank defects. This follows by 2 rank deficiencies solved by the GPS (G) hardware (HW) code delays on frequencies $j = 1, 2$ for $r = 2$ $\left(d_{2,1}^G, d_{2,2}^G \right)$, and $m_G + m_*$ rank defects solved by the ionospheric delays for $r = 1$, all satellites and all systems $(\iota_1^{s_G}, \iota_1^{s_*})$. Then there are $3 \cdot 1$ (3 corresponds to 3 additional systems to GPS) rank defects solved by the HW code delays on $j = 1$, $r = 2$ for system $*$ $\left(d_{2,1}^* \right)$, and $2f + 3 \cdot 2f$ rank defects solved by the HW code $\left(d_{1,j}^G, d_{1,j}^* \right)$ and phase delays $\left(\delta_{1,j}^G, \delta_{1,j}^* \right)$, on $j = 1, \ldots, f$, $r = 1$ and for all systems. Further rank defects of size $f + 3 \cdot f$ are solved by fixing the ambiguities on $j = 1, \ldots, f$, $r = 2$ and for the pivot satellites $s_G = 1_G$, $s_* = 1_*$ $\left(z_{2,j}^{1_G}, z_{2,j}^{1_*} \right)$, and a rank deficiency of size $fm_G + fm_*$ that are solved by fixing the ambiguities on $j = 1, \ldots, f$, $r = 1$, for all satellites and systems $\left(z_{1,j}^{s_G}, z_{1,j}^{s_*} \right)$. For more details about the rank defects solved by the S-basis in Table 2, see Appendix A.

The ISBs-float full-rank system of observation equations for the combination of GPS+BDS+Galileo+QZSS on overlapping frequencies $j = 1, \ldots, f$ then read,

$$p_{12,j}^{s_G} = -g_2^{s_G T} \Delta x_{12} + m_2^{s_G} \tilde{\tau}_{12} + d\tilde{t}_{12} + \tilde{d}_{12,j}^G + \mu_j \tilde{\iota}_{12}^{s_G}$$

$$\phi_{12,j}^{s_G} = -g_2^{s_G T} \Delta x_{12} + m_2^{s_G} \tilde{\tau}_{12} + d\tilde{t}_{12} + \tilde{\delta}_{12,j}^G - \mu_j \tilde{\iota}_{12}^{s_G} + \\ + \lambda_j \tilde{z}_{12,j}^{1_G s_G}$$

$$p_{12,j}^{s_*} = -g_2^{s_* T} \Delta x_{12} + m_2^{s_*} \tilde{\tau}_{12} + d\tilde{t}_{12} + \tilde{d}_{12,j}^G + \tilde{d}_{12,j}^{G*} + \mu_j \tilde{\iota}_{12}^{s_*}$$

$$\phi_{12,j}^{s_*} = -g_2^{s_* T} \Delta x_{12} + m_2^{s_*} \tilde{\tau}_{12} + d\tilde{t}_{12} + \tilde{\delta}_{12,j}^G + \tilde{\delta}_{12,j}^{G*} - \mu_j \tilde{\iota}_{12}^{s_*} + \\ + \lambda_j \tilde{z}_{12,j}^{1_* s_*}$$

$$(1)$$

The estimable unknown parameters, denoted with a 'tilde', are given in Table 3, and the notations used in (1) are further described in Table 4.

Table 3: Estimable unknown parameters and their interpretation for the ISBs-float model (1)

Notation and interpretation	Estimable parameter	Conditions
$\Delta x_{12} = \Delta x_2 - \Delta x_1$	relative receiver coordinates	$r \geq 2$
$\tilde{\tau}_{12} = \tau_2 - \tau_1$	relative (residual) wet ZTD	$r \geq 2$
$d\tilde{t}_{12} = dt_{12} + \frac{\mu_2}{\mu_2-\mu_1}d^G_{12,1} - \frac{\mu_1}{\mu_2-\mu_1}d^G_{12,2}$	relative receiver clock with GPS HW code delays on $j=1,2$	$r \geq 2$
$\tilde{d}^G_{12,j} = d^G_{12,j} - \frac{\mu_2-\mu_j}{\mu_2-\mu_1}d^G_{12,1} + \frac{\mu_1-\mu_j}{\mu_2-\mu_1}d^G_{12,2}$	relative GPS receiver HW code delays	$j \geq 3, r \geq 2$
$\tilde{\delta}^G_{12,j} = \delta^G_{12,j} - \frac{\mu_2+\mu_j}{\mu_2-\mu_1}d^G_{12,1} + \frac{\mu_1+\mu_j}{\mu_2-\mu_1}d^G_{12,2} + \lambda_j z^{1_G}_{12,j}$	relative GPS receiver HW phase delays	$j \geq 1, r \geq 2$
$\tilde{d}^{G*}_{12,j} = d^{G*}_{12,j} - \frac{\mu_j}{\mu_1}d^{G*}_{12,1}$	relative code inter-system bias (ISB)	$j \geq 2, r \geq 2$
$\tilde{\delta}^{G*}_{12,j} = \delta^{G*}_{12,j} + \frac{\mu_j}{\mu_1}d^{G*}_{12,1} + \lambda_j z^{1_G 1_*}_{12,j}$	relative phase ISB biased by inter-system double-differenced ambiguities	$j \geq 1, r \geq 2$
$\tilde{\iota}^{sG}_{12} = \iota^{sG}_{12} + \frac{1}{\mu_2-\mu_1}\left(d^G_{12,2} - d^G_{12,1}\right)$	relative GPS slant ionospheric delays	$r \geq 2, s \geq 1$
$\tilde{\iota}^{s*}_{12} = \iota^{s*}_{12} + \frac{1}{\mu_2-\mu_1}\left(d^G_{12,2} - d^G_{12,1}\right) + \frac{1}{\mu_1}d^{G*}_{12,1}$	relative system $*$ slant ionospheric delays biased by GPS differential code biases (DCBs) and code ISB on $j=1$	$r \geq 2, s \geq 1$
$\tilde{z}^{1_G s_G}_{12,j} = z^{s_G}_{12,j} - z^{1_G}_{12,j}$	GPS double-differenced integer ambiguities	$j \geq 1, r \geq 2, s \geq 2$
$\tilde{z}^{1_* s_*}_{12,j} = z^{s_*}_{12,j} - z^{1_*}_{12,j}$	system * double-differenced integer ambiguities	$j \geq 1, r \geq 2, s \geq 2$

Table 4: Definition of commonly used symbols

Symbol	Definition	Description
r	$=1,2$	receivers used
s	$=1,\ldots,m$	tracked satellites
$G, *$		systems, G for GPS, $*$ equals B BDS, E Galileo and Q QZSS
j	$=1,\ldots,f$	tracked overlapping frequencies
$(\cdot)_{12}$	$=(\cdot)_2 - (\cdot)_1$	between-receiver SDs
$(\cdot)^{1s}$	$=(\cdot)^s - (\cdot)^1$	between-satellite SDs
$p^s_{12,j}, \phi^s_{12,j}$		SD code and phase observables respectively
g^{sT}_r	$=\frac{(x^s-x_r)^T}{||x^s-x_r||}$	line-of-sight unit vector
$(.)^T$		transpose of vector
$||.||$		norm
x^s, x_r		vector of satellite and receiver coordinates respectively
λ_j		wavelength for frequency j
m^r_r		mapping function to get a station-wise (wet) ZTD
μ_j	$=f^2_1/f^2_j$	conversion of ionospheric delay from GPS $L1$ to frequency j
$d^{G*}_{12,j}$	$=d^*_{12,j} - d^G_{12,j}$	code inter-system bias (ISB)
$\delta^{G*}_{12,j}$	$=\delta^*_{12,j} - \delta^G_{12,j}$	phase ISB

The Saastamoinen troposphere model has been used to correct the dry part of the troposphere [18] in (1), and we refrain from carrying through SD random observation noise and other systematic effects such as multipath for notational convenience. The shared parameters between GPS and system $*$ in (1) are the receiver coordinates Δx_{12}, relative ZTD $\tilde{\tau}_{12}$, receiver clock $d\tilde{t}_{12}$ and the GPS HW code/phase delays $\tilde{d}^G_{12,j}, \tilde{\delta}^G_{12,j}$. The estimable double-differenced integer ambiguities in Table 3 are differenced with respect to the ambiguities of a system-specific pivot satellite, respectively. Note that the observation equations in (1) has equivalent redundancy to taking a traditional system-specific receiver clock model as the code ISBs are estimable on the second frequency and beyond, whereas the GPS receiver HW code delays are only estimable for $j \geq 3$. Thus the code ISBs play the role of the additional unknowns instead of additional receiver clocks.

One can also make use of a re-parameterization of the code/phase ISBs and GPS receiver HW code/phase delays to get system-specific HW delays for non-overlapping frequencies,

$$\tilde{d}^*_{12,j_*} = \tilde{d}^{G*}_{12,j} + \tilde{d}^G_{12,j} =$$
$$= d^*_{12,j} - \frac{\mu_2-\mu_j}{\mu_2-\mu_1}d^G_{12,1} + \frac{\mu_1-\mu_j}{\mu_2-\mu_1}d^G_{12,2} - \frac{\mu_j}{\mu_1}d^{G*}_{12,1}$$
$$\tilde{\delta}^*_{12,j} = \tilde{\delta}^{G*}_{12,j} + \tilde{\delta}^G_{12,j} =$$
$$= \delta^*_{12,j} - \frac{\mu_2+\mu_j}{\mu_2-\mu_1}d^G_{12,1} + \frac{\mu_1+\mu_j}{\mu_2-\mu_1}d^G_{12,2} + \frac{\mu_j}{\mu_1}d^{G*}_{12,1} + \lambda_j z^{1_*}_{12,j}$$

(2)

i.e. the delays are now relative to the GPS HW code delays on frequency $j = 1,2$, and the receiver HW phase delays are now solely biased by its own system-specific pivot satellite 1 ambiguity (compare to the phase ISBs in Table 3). More importantly this re-parameterization (2) shows that the full-rank ISBs-float model in (1) is equivalent, in terms of redundancy, to the one where one would choose to parameterize system-specific HW delays.

ISBs-fixed, ionosphere-float functional model

In the previous section it was shown that if we for overlapping frequencies parameterize the ISBs, it does not strengthen the model as compared to a traditional model with system-specific receiver clocks/HW delays. We will refer to the following model (7) as the "ISBs-fixed model", where the ISBs will be assumed completely known (deterministic) and thus subtracted from the code/phase observations.

The code and phase ISBs in the observation equations (1) to be corrected, denoted with a 'tilde', are defined as,

$$\tilde{d}^{G*}_{12,j} = d^{G*}_{12,j} - \frac{\mu_j}{\mu_1}d^{G*}_{12,1}$$
$$\tilde{\delta}^{G*}_{12,j} = \delta^{G*}_{12,j} + \frac{\mu_j}{\mu_1}d^{G*}_{12,1} + \lambda_j z^{1_G 1_*}_{12,j}$$

(3)

respectively (see Table 3). Now consider the case where we want to determine these ISBs using another data set. The code and phase ISB corrections, denoted with 'overline', can be given as [11],

$$
\begin{aligned}
\overline{d}_{12,j}^{G*} &= \tilde{d}_{12,j}^{G*} \\
\overline{\delta}_{12,j}^{G*} &= \delta_{12,j}^{G*} + \frac{\mu_j}{\mu_1} d_{12,1}^{G*} + \lambda_j a_{12,j}
\end{aligned}
\tag{4}
$$

respectively, where $a_{12,j} \in \mathbb{Z}$ is an integer ambiguity that in principle is different from $z_{12,j}^{1_G 1_*}$ in the observations that we would like to correct (1). This since the observations used to determine the corrections in (4) are also different. The phase ISBs corrections can thus be re-written as,

$$
\overline{\delta}_{12,j}^{G*} = \tilde{\delta}_{12,j}^{G*} - \lambda_j \left(z_{12,j}^{1_G 1_*} - a_{12,j} \right)
\tag{5}
$$

Consequently when the correction (5) is applied to the phase observations of system * in (1), the ambiguity difference in (5) will be lumped into the ambiguities $\tilde{z}_{12,j}^{1_* s_*}$ (Table 3) as,

$$
z_{12,j}^{1_G s_*} = z_{12,j}^{1_* s_*} + \left(z_{12,j}^{1_G 1_*} - a_{12,j} \right) = z_{12,j}^{1_G s_*} - a_{12,j}
\tag{6}
$$

i.e. the ambiguity of system * (6) is now differenced with respect to the pivot satellite of GPS minus the integer ambiguity $a_{12,j}$. It is thus not problematic that there is an additional ambiguity $a_{12,j}$ since it is only the combined integer ambiguity term $\tilde{z}_{12,j}^{1_G s_*}$ that is estimable.

The full-rank ISBs-fixed system of observation equations on overlapping frequencies $j = 1, \ldots, f$ can be expressed as follows,

$$
\begin{aligned}
p_{12,j}^{s_G} &= -g_2^{s_G T} \Delta x_{12} + m_2^{s_G} \tilde{\tau}_{12} + d\tilde{t}_{12} + \tilde{d}_{12,j}^{G} + \mu_j \tilde{\iota}_{12}^{s_G} \\
\phi_{12,j}^{s_G} &= -g_2^{s_G T} \Delta x_{12} + m_2^{s_G} \tilde{\tau}_{12} + d\tilde{t}_{12} + \tilde{\delta}_{12,j}^{G} - \mu_j \tilde{\iota}_{12}^{s_G} + \\
&\quad + \lambda_j \tilde{z}_{12,j}^{1_G s_G} \\
p_{12,j}^{s_*} - \overline{d}_{12,j}^{G*} &= -g_2^{s_* T} \Delta x_{12} + m_2^{s_*} \tilde{\tau}_{12} + d\tilde{t}_{12} + \tilde{d}_{12,j}^{G} + \mu_j \tilde{\iota}_{12}^{s_*} \\
\phi_{12,j}^{s_*} - \overline{\delta}_{12,j}^{G*} &= -g_2^{s_* T} \Delta x_{12} + m_2^{s_*} \tilde{\tau}_{12} + d\tilde{t}_{12} + \tilde{\delta}_{12,j}^{G} - \mu_j \tilde{\iota}_{12}^{s_*} + \\
&\quad + \lambda_j \tilde{z}_{12,j}^{1_G s_*}
\end{aligned}
\tag{7}
$$

where the ambiguity $\tilde{z}_{12,j}^{1_G s_*}$ for system * (6) will also be estimable for $s_* = 1_*$. This gives us f additional unknowns for each system added to GPS as compared to the ISBs-float model. However, since we also have a-priori corrections for the code $(f-1)$ and phase ISBs (f) that gives us $2f-1$ corrections, the redundancy of the model (7) increases with $f-1$ for each additional system to GPS as compared to the ISBs-float model (1). In other words at least $f \geq 2$ overlapping frequencies for each additional system is required to strengthen the ionosphere-float model accordingly. This is further clarified by Table 5. Note finally that the other unknown parameters in

(7) and their interpretations are given in Table 3, and that the GPS observation equations are still equivalent to the ISBs-float case (1).

Stochastic models

The variance-covariance (VCV) matrix of the code and phase observables in SD form, for a single-system and the ionosphere-float model can be given as,

$$
Q_{yy}^* = \text{blkdiag}\left(C_p^*, C_\phi^* \right) \otimes \left(D_n^T D_n \otimes W_{m_*}^{-1} \right)
\tag{8}
$$

where 'blkdiag' denoted a blockdiagonal matrix, $\otimes$ is the Kronecker product [19], and the a priori variance factors of the code and phase observables are given in the sub-matrices $C_p^* = \text{diag}(\sigma_{p,1_*}^2, \ldots, \sigma_{p,f_*}^2)$ and $C_\phi^* = \text{diag}(\sigma_{\phi,1_*}^2, \ldots, \sigma_{\phi,f_*}^2)$ respectively. We assume no cross-correlation between code and phase nor between frequencies, otherwise the non-diagonal elements of C_p^* and C_ϕ^* would be populated accordingly with covariances between the observables. We also have D_n^T with -1 for the pivot receiver and a 1 for the second receiver that is the between-receivers SD operator [20], and $W_{m_*}^{-1}$ contains the elevation-dependent weighting function as given by [21]. The combined GPS+BDS+Galileo+QZSS ionosphere-float (1), (7) VCV-matrix reads,

$$
Q_{yy} = \text{blkdiag}\left(Q_{yy}^G, Q_{yy}^B, Q_{yy}^E, Q_{yy}^Q \right)
\tag{9}
$$

Redundancy and solvability condition

The redundancy is computed as the number of observations minus the number of estimable unknowns, which is given in Table 5 for the instantaneous single-baseline RTK ISBs-float (1) and ISBs-fixed (7) models respectively. In the last column a "solvability condition" is given, which is the number of satellites required to solve the models. Note that in this contribution we will have two systems that have the required number of overlapping frequencies $f \geq 2$ that allow for strengthening of the ISBs-fixed model in comparison to the ISBs-float counterpart, namely GPS/QZSS L1,L2 (Table 1). Thus when presenting the ISBs-fixed redundancy/solvability condition in Table 5, we take only these ISBs into account. The single-system model in Table 5 can be found in (1) and (7) for GPS, whereas BDS, Galileo and QZSS only models will have a similar definition of the unknowns. The dynamic model used for the Kalman filter to strengthen the instantaneous RTK models is briefly explained in the following section.

For the single-system in Table 5 we have: 3 receiver coordinates, 1 ZTD, 1 receiver clock, $(f_* - 2)$ receiver HW code delays, f_* receiver HW phase delays, m_* slant ionospheric delays and $f_*(m_* - 1)$ double-differenced integer ambiguities to estimate. More importantly the required number of frequencies and satellites to solve the

Table 5: Single-baseline instantaneous RTK: number of observations, unknowns, redundancy and solvability condition for the (ionosphere-float, ZTD-float) ISBs-float (1) and ISBs-fixed (7) models on overlapping frequencies of L1,L2 GPS/QZSS

Model	# of observations	# of unknowns	Redundancy	Solvability condition
				$f \geq 2$
Single-system (1)	$2f_* m_*$	$3 + f_* + m_* + f_* m_*$	$f_*(m_* - 1) - m_* - 3$	$m_* \geq 5$
4-system ISBs-float (1)	$2fm_G+$ $+2f_B m_B$ $+2f_E m_E$ $+2fm_Q$	$f + m_G + fm_G+$ $+f_B + m_B + f_B m_B$ $+f_E + m_E + f_E m_E$ $+f + m_Q + fm_Q$	$f(m_G - 1) - m_G+$ $+f_B(m_B - 1) - m_B$ $+f_E(m_E - 1) - m_E$ $+f(m_Q - 1) - m_Q$	$m_G + m_B+$ $+m_E + m_Q \geq 8$
4-system ISBs-fixed (7) (QZSS-GPS)	$2fm_G+$ $+2f_B m_B$ $+2f_E m_E$ $+2fm_Q$	$1 + f + m_G + fm_G+$ $+f_B + m_B + f_B m_B$ $+f_E + m_E + f_E m_E$ $+m_Q + fm_Q$	$f(m_G - 1) - m_G+$ $+f_B(m_B - 1) - m_B$ $+f_E(m_E - 1) - m_E$ $+fm_Q - m_Q - 1$	$m_G + m_B+$ $+m_E + m_Q \geq 7$

Figure 2: Satellite visibility for GPS, BDS, Galileo and QZSS with 20° cut-off angle in Perth (Muresk), 8 hours in February 19, 2014. At *top* we have the total # of satellites for GPS, BDS, Galileo and QZSS. At *bottom* the redundancies (Table 5) for the instantaneous single-baseline RTK models are given as well. The L1,L2 QZSS-GPS code/phase ISBs are assumed fixed for the ISBs-fixed (7) models

single-system model is two and five respectively. For the 4-system ISBs-float and ISBs-fixed models eight and seven satellites are required respectively. In other words the positioning flexibility is increased in comparison to the single-system, where two satellites for each system would be sufficient to solve the model in the ISBs-float case (minus one satellite for the ISBs-fixed counterpart). Whereas having the same number of satellites using any of the systems separately would not be sufficient to solve the model.

We give in Figure 2 the number of satellites (top) and the redundancies in Table 5 (bottom) for a station in Perth (Muresk), as a function over almost 8 hours of real data. This is given between 13:16:30-21:11:30 local Perth time, February 19, 2014, and for an elevation cut-off angle of 20°. This time period is selected since the satellites from all four systems are visible at the same time instances, see also Figure 1. The higher cut-off angle is depicted as to illustrate an urban canyon like environment or when any existing low-elevation multipath is preferably avoided. The redundancies are depicted as to illustrate the reliability of the dual-frequency GPS (blue), GPS+Galileo+QZSS (green) and four-system (black) RTK models. The ISBs-float models are denoted with dashed lines, whereas the ISBs-fixed models are given by full-lines. Reliability is a measure of the ability of the system to test the observations for modeling errors, and zero redundancy gives infinitely poor reliability as testing is then not possible.

Figure 2 illustrates that GPS-only have zero redundancy 14.2% of all epochs, whereas when Galileo and QZSS is added the redundancy is larger than zero throughout the whole time-period. One can also observe that the GPS+Galileo+QZSS ISBs-float model (dashed green line) is equivalent to GPS (blue line) when one Galileo and one QZSS satellite is visible, respectively. However for the ISBs-fixed counterpart (full green line) the redundancy immediately increases with one ($f - 1$, with $f = 2$), since the L1,L2 QZSS-GPS code/phase ISBs
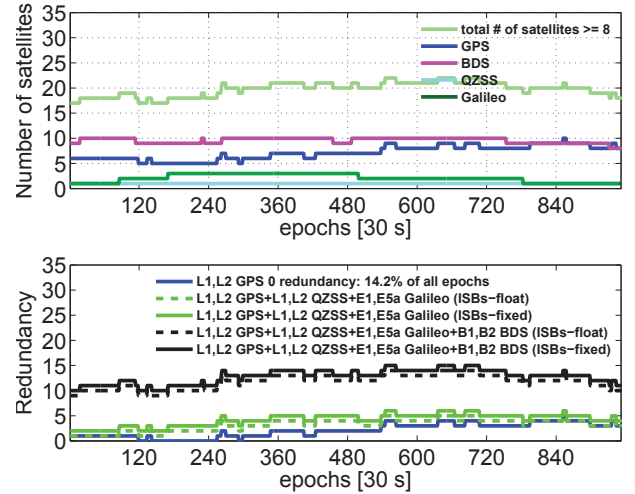
are then fixed. A significant increase in redundancy can also be seen when BDS is added to the three other systems (black lines). This thus indicates the possibility of using higher satellite elevation cut-off angles when combining the systems and still retain sufficient redundancy.

Dynamic model for the Kalman filter

The unknowns in the observation equations for the ionosphere-float models (1) and (7) can be estimated using an extended Kalman filter with a dynamic model. The state vector for which a dynamic model will be used can be expressed in vector form for epoch $i = 1, \ldots, k$ as follows,

$$x(i) = \left[\tilde{\tau}_{12}(i), z_{12}^T(i) \right]^T \qquad (10)$$

where we have $\tilde{\tau}_{12}(i)$ the relative (wet) ZTD and the ambiguities in a vector $z_{12}(i) = \left[z_{12}^{G\,T}(i), z_{12}^{B\,T}(i), z_{12}^{E\,T}(i), z_{12}^{Q\,T}(i) \right]^T$, with $z_{12}^*(i) = \left[z_{12,1_*}^{*\,T}(i), \ldots, z_{12,f_*}^{*\,T}(i) \right]^T$ and $z_{12,j_*}^*(i) = \left[\tilde{z}_{12,j_*}^{1_* 2_*}(i), \ldots, \tilde{z}_{12,j_*}^{1_* m_*}(i) \right]^T$. For the ISBs-fixed model (7) the ambiguities for QZSS will read $z_{12,j}^Q(i) = \left[\tilde{z}_{12,j}^{1_G 1_Q}(i), \ldots, \tilde{z}_{12,j}^{1_G m_Q}(i) \right]^T$, i.e. f additional ambiguities (relative to the GPS pivot satellite 1_G) need to be included in the state vector in comparison to the ISBs-float model.

The dynamic model used for the extended Kalman filter follows as,

$$x_k = \Phi_{k|k-1} x_{k-1} + d_k,$$
$$D(d_k) = Q_{d_k} \tag{11}$$

where x_k is the state vector at epoch k connected with the state vector at previous epoch $k-1$, x_{k-1}, by $\Phi_{k|k-1}$ the transition matrix, d_k the process noise with zero mean and VCV-matrix Q_{d_k}, where $D(\cdot)$ is the dispersion. All other parameters (Table 3) are assumed unlinked in time.

The transition matrix for the ISBs-float model is then defined as,

$$\Phi_{k|k-1} = \text{blkdiag}(1, I_n) \tag{12}$$

where 1 corresponds to the ZTD and I_n is the identity matrix of the size $n = f(m_G - 1) + f_B(m_B - 1) + f_E(m_E - 1) + f(m_Q - 1)$ corresponding to the ambiguities. Note that n has an additional size of $+f$ for the ISBs-fixed model (corresponding to the QZSS satellite 1 ambiguities). The process noise VCV-matrix follows as,

$$Q_{d_k} = \text{blkdiag}(\Delta t \cdot q_{\mathfrak{r}}, 0_n) \tag{13}$$

where Δt is the time-interval between adjacent epochs, $q_{\mathfrak{r}}$ is the spectral density for the relative (wet) ZTD that is modeled as random walk, and 0_n is the zero matrix of dimension n used for the ambiguities since they are treated as time-constant. The dynamic model settings are given in Table 6.

GNSS DATA COLLECTION

The Trimble NetR9 receivers/antennas used to form the baseline analyzed in this contribution is depicted in Figure 1 and Figure 3, with a baseline length of 80 km. The station CUT0 is located in Bentley, Perth and at the Curtin University campus, whereas station MURT is located in Muresk. The number of satellites for a GPS+BDS+Galileo+QZSS system and an elevation cut-off angle of $10°$ is presented in Figure 3 as well. We see more than double the number of satellites for the combination of the four systems in comparison to GPS as a stand alone system. In this contribution we will focus on the data in February 19, 2014 between 12:34:30-21:40:30 local Perth time, i.e. for a time span of 9 hours and 6 minutes, as all four satellite systems are then continuously tracked over the day for the $10°$ cut-off angle.

For all of the following analyzes we use a measurement interval of 30 s. The Detection, Identification and Adaptation (DIA) procedure is utilized to detect, identify and adapt for outliers [22], and the LAMBDA method [23] for integer ambiguity resolution. Note that the dual-frequencies of GPS/QZSS L1,L2, Galileo E1,E5a and

(a) CUT0 (*left*) (Bentley) and MURT (*right*) (Muresk) antennas
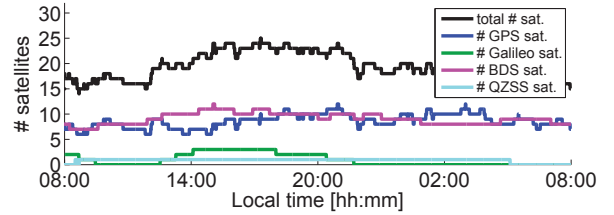
(b) # of satellites for a cut-off angle of $10°$ in Muresk, and period of analysis 12:34:30-21:40:30 local Perth time

Figure 3: GNSS Trimble NetR9 receivers/antennas for single-baseline RTK in February 19, 2014

BDS B1,B2 will be analyzed throughout this contribution (Table 1), and that the E5a frequency of the E11 satellite could not be tracked for this data set thus three out of four Galileo IOV satellites will be used.

DYNAMIC/STOCHASTIC MODEL SETTINGS

In Table 6 we present the functional models that are investigated and the corresponding dynamic model settings (13) for the Kalman filter solutions. The ambiguities are treated as time-constant and a random walk process noise of $2\,\text{mm}/\sqrt{\text{hour}}$ is used for the relative ZTD prediction. This process noise was predicted similarly to Chapter 3.4.3 in [24], as determined from data independent from the data analyzed in this contribution.

Table 6: Dynamic model settings (13). Epoch-by-epoch (ebe) denotes no linkage in time when estimating the parameters

Model	Mode	Dynamic model	Process noise
Iono-float (1),(7)	Single-epoch	All parameters: ebe	-
Iono-float (1),(7)	Kalman filter	Ambiguities time-constant: Relative ZTD random walk: Other parameters: ebe	0 $2\,\text{mm}/\sqrt{\text{hour}}$ -

The stochastic model (9) settings are depicted in Table 7. This is based on the exponential elevation weighting function by [21] and zenith-referenced a priori code and phase standard deviations (STDs) respectively for undifferenced observations.

Table 7: Zenith-referenced code and phase STDs (9) for the Trimble NetR9 receivers in Figure 3

System	Frequency	Code $\sigma_{P,_{js}}$ [cm]	Phase $\sigma_{\phi,_{js}}$ [mm]
GPS	L1	30	2
	L2	30	2
BDS	B1	30	2
	B2	30	2
Galileo	E1	30	2
	E5a	30	2
QZSS	L1	30	2
	L2	30	2

FORMAL ANALYSIS OF FOUR-SYSTEM SINGLE-BASELINE RTK MODEL

In this section a formal analysis will be conducted for the four-system ionosphere-float, ZTD-float RTK models. For the following computations we only need the design matrix and VCV-matrix of the observations, i.e. real data is not necessary.

Ambiguity Dilution of Precision

Ambiguity Dilution of Precision (ADOP) is a scalar measure of the model strength for ambiguity resolution and was introduced in [20]. The ADOP is defined as,

$$\text{ADOP} = \sqrt{|Q_{\hat{a}\hat{a}}|^{\frac{1}{n}}} \quad [\text{cycle}] \qquad (14)$$

where $Q_{\hat{a}\hat{a}}$ is the variance-covariance (VCV) matrix of the float ambiguities, $|\cdot|$ is the determinant, and n is the dimension of the ambiguity vector. The ADOP measures the intrinsic precision of the ambiguities, and is also a measure of the volume of the ambiguity confidence ellipsoid [25]. As a rule-of-thumb, an ADOP of 0.12 cycle can be taken as indication of successful ambiguity resolution as it corresponds to an ambiguity success rate (SR) larger than 99.9% [26]. Our earlier studies [8],[27] show that successful instantaneous single-frequency L1+B1 GPS+BDS RTK is feasible for baselines of a few km when the relative atmospheric delays are negligible, whereas dual-frequencies were needed when using any of the systems separately. For a medium baseline length of 17 km, when the uncertainty of the relative ionospheric pseudo-observables can be modeled as a function of the baseline length [28], we found that successful instantaneous dual-frequency L1,L2+B1,B2 GPS+BDS RTK is possible.

To investigate whether successful *instantaneous* dual-frequency ionosphere-float RTK is feasible as well, Figure 4 depicts the single-epoch ADOP time-series in blue for 9 hours of data (see Figure 3). The ADOPs for GPS are given at top, GPS+Galileo+QZSS ISBs-float and ISBs-fixed at the second and third rows respectively, and at the fourth row the four-system ISBs-fixed model is depicted as well. An elevation cut-off angle of 10° is used,

and an ADOP-level of 0.12 cycle is indicated by a dashed red line. The number of satellites is depicted at bottom.

The single-epoch ADOP time-series of GPS in Figure 4 is larger than when combining GPS with Galileo, QZSS and/or BDS due to the fewer number of satellites. One can also see for the GPS+Galileo+QZSS ISBs-float model that once two Galileo satellites are tracked, just before 120 epochs have passed, the ADOPs decrease in comparison to GPS. The single QZSS satellite is furthermore only contributing throughout the whole time period when the L1,L2 QZSS-GPS code/phase ISBs are assumed fixed. This is also shown by the redundancies in Table 5 and in Figure 2. More importantly the combination of all four-systems provides for the smallest ADOPs with a mean value of 0.42 cycles, which is, however, larger than the 0.12 cycle level we need to expect successful ambiguity resolution.

Thus we will now investigate the ADOPs using a *Kalman filter* with the dynamic model in Table 6, and the ADOPs are depicted in Figure 5 corresponding to the time-period in Figure 4. The GPS model is given at top and the four-system model at bottom. Note that the ADOP is computed based on the Kalman filtered VCV-matrix of the ambiguities, thus as more time passes the stronger the model becomes (since the float ambiguities become more precise). A zoom-in is therefore given for the first 60 epochs (30 minutes) to illustrate the time to reach the 0.12 cycle level.

The combined GPS+Galileo+QZSS+BDS system in Figure 5 is seen to converge to ADOP levels of 0.12 cycles much quicker than GPS due to larger redundancy of the model. This is a very promising first indication that faster successful ambiguity resolution is possible for the ionosphere-float model when combining the systems.

Positioning

In the following positioning results we will investigate full ambiguity resolution for Kalman filter based dual-frequency GPS+BDS+Galileo+QZSS RTK models. In the previous section it was namely concluded that a Kalman filter is needed for the ionosphere-float model to achieve successful ambiguity resolution.

A formal bootstrapped success rate (SR) criterion will be used to decide when to fix the ambiguities, to allow the float ambiguities to converge. The formal bootstrapped SR is an accurate lower bound to the integer least-squares (ILS) SR [29, 30], and follows as,

$$P[\check{z}_{IB} = z] = \prod_{i=1}^{n} \left[2\Phi\left(\frac{1}{2\sigma_{\hat{z}_{i|I}}}\right) - 1 \right] \geq P_0 \qquad (15)$$
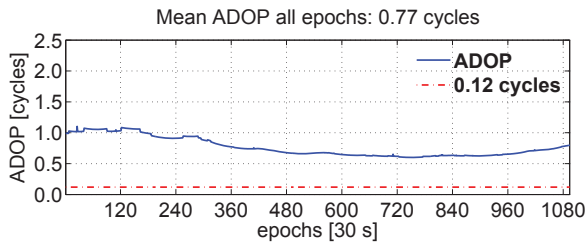
where $P[\check{z}_{IB} = z]$ denotes the probability of correct integer estimation of the integer bootstrapped estimator $\check{z}_{IB}$,
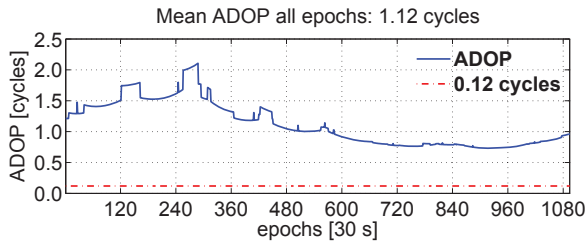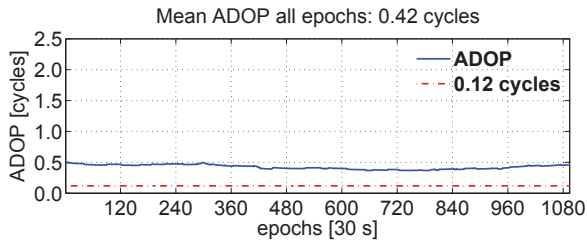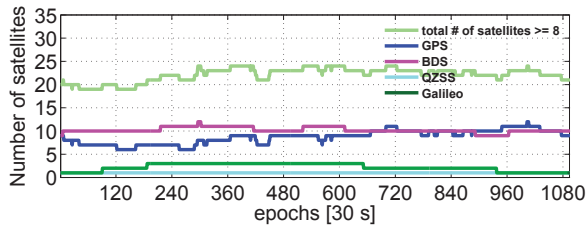
(a) L1,L2 GPS
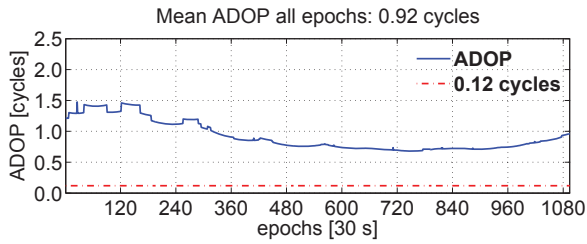
(b) ISBs-float: L1,L2+E1,E5a+L1,L2 GPS+Galileo+QZSS

(c) ISBs-fixed: L1,L2+E1,E5a+L1,L2 GPS+Galileo+QZSS
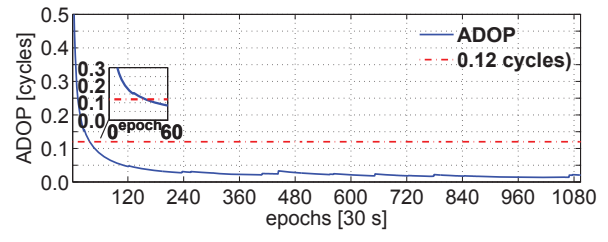

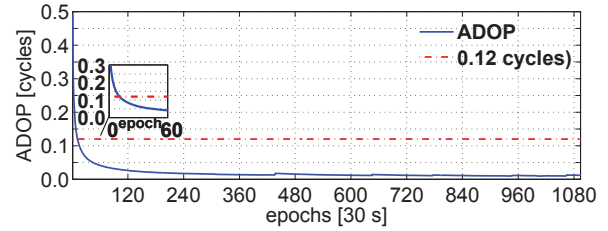
(d) ISBs-fixed: L1,L2+E1,E5a+L1,L2+B1,B2 GPS+Galileo+QZSS+
+BDS

(e) Number of satellites

Figure 4: Ionosphere-float, ZTD-float *single-epoch* ADOP time-series (*blue*) for single-baseline RTK, using $10°$ cut-off angle. *Light green* represents the total # of satellites. February 19, 2014, and 9 hours of data. The L1,L2 QZSS-GPS code/phase ISBs are assumed fixed for the ISBs-fixed models

(a) L1,L2 GPS

(b) ISBs-fixed: L1,L2+E1,E5a+L1,L2+B1,B2 GPS+Galileo+QZSS+
+BDS

Figure 5: Ionosphere-float, ZTD-float *Kalman filter* ADOP time-series (*blue*) for single-baseline RTK, using $10°$ cut-off angle. February 19, 2014, and 9 hours of data. The L1,L2 QZSS-GPS code/phase ISBs are assumed fixed

$\Phi(x) = \int_{-\infty}^{x} \frac{1}{\sqrt{2\pi}} exp\left(-\frac{1}{2}v^2\right) dv$ is the cumulative normal distribution, $\sigma_{\hat{z}_{i|I}}$ with $i = 1, \dots, n$, $I = 1, \dots, (i-1)$ is the conditional STDs of the decorrelated ambiguities and P_0 a user-defined bootstrapped success criterion. A value of $P_0 = 99.9\%$ will be used, and if it is not fulfilled we take the float solution instead. This criterion (15) will also decide upon when to include newly risen satellites. The satellites are considered to rise when they exceed the user-defined elevation cut-off angle of e.g. $10°$.

In the following we will compute the average ambiguity convergence time, also referred to as time to first fix (TTFF), to fulfill the criterion in (15). The Kalman filter is initialized at the first-epoch, and for each additional epoch included in the filter the bootstrapped SR criterion in (15) is used. Once it reaches 99.9% we obtain the TTFF. Then we re-initialize the filter at the second epoch and the whole procedure is repeated again. The times given in Table 8 are the mean of all these TTFFs over approximately 9 hours in February 19, 2014 for a $10°$ elevation cut-off angle. The corresponding expected positioning precision in terms of formal STDs in local North (N), East (E), Up (U) of the float and fixed dual-frequency ionosphere-float, ZTD-float solutions are also given in Table 8. The results are given for GPS, GPS+Galileo+QZSS and GPS+Galileo+QZSS+BDS.

Since the ambiguities are treated as time-constant parameters and random walk process noise is used for the relative ZTD in the dynamic model (Table 6), the

Table 8: Formal STDs for ionosphere-float, ZTD-float dual-frequency RTK and a cut-off angle of 10°, ambiguity float/fixed solutions in North, East and Up. The L1,L2 QZSS-GPS code/phase ISBs are assumed fixed (and within brackets the ISBs-float case is given as well). The STDs are mean values of all formal STDs based on re-initializations of the Kalman filter during 9 hours in February 19, 2014 and when the boot-strapped SR in (15) of 99.9% is fulfilled. In the last column the corresponding # of epochs needed is depicted as well.

System/frequency	Formal STDs float/fixed			# epochs
	N [cm]	E [cm]	U [cm]	[30 s]
L1,L2 GPS	5.9/1.0	14.9/0.9	15.3/2.5	41
L1,L2+E1,E5a+L1,L2	5.8/0.8	11.8/0.7	14.0/2.2	32
GPS+Galileo+QZSS	(5.8/0.9)	(13.2/0.8)	(13.9/2.4)	36
L1,L2+E1,E5a+L1,L2+B1,B2	4.5/0.6	8.0/0.5	10.4/1.7	28
GPS+Galileo+QZSS+BDS	(4.5/0.6)	(8.3/0.5)	(10.4/1.8)	29

ambiguity-float position STDs improve with respect to time. Table 8 illustrates the improvement when going from ambiguity-float to ambiguity-fixed solutions as well as the improvement which a combination of the systems brings. The improvement in ambiguity-float East and Up components are more significant than in the North component. More importantly the combined systems provides for the ambiguity-float precisions in Table 8 earlier (smaller TTFF) than for GPS. Thus when combining the systems we can potentially achieve *faster* ambiguity-float precisions at the dm-level and *faster* availability to ambiguity-fixed positioning precisions at the mm-cm-level. This is particularly true when the L1,L2 QZSS-GPS code/phase ISBs are assumed fixed and/or when BDS is added to the three other systems. We will elaborate more on this in the empirical positioning section. One can finally note in Table 8 that the East component experience larger improvements in comparison to the North and Up components when integer-ambiguity resolution is applied, which is consistent with e.g. [31, 32].

EMPIRICAL ANALYSIS OF FOUR-SYSTEM SINGLE-BASELINE RTK MODEL

In this section real data will be analyzed as to verify the formal claims in the previous sections. The L1,L2 QZSS-GPS code/phase ISBs will safely be taken as zero throughout the analysis for the similar Trimble NetR9 receiver types in Figure 3, see e.g. [15]. The BDS GEO ambiguities are kept as float parameters in the following sections due to site-specific multipath effects in combination with the satellites being stationary [33]. Thus any systematic effects from the GEO satellites cannot be significantly mitigated over time and was shown to negatively affect the ambiguity resolution performance.

Positioning

Table 9 provides the empirical float and correctly fixed ionosphere-float, ZTD-float positioning precision for dual-frequency GPS, GPS+Galileo+QZSS and GPS+Galileo+QZSS+BDS. This is given for a 10° elevation cut-off angle, and the STDs were obtained by comparing the estimated positions to precise benchmark coordinates. These computations are based on the re-initializations of the Kalman filter and the bootstrapped SR criterion (15), similar to the formal STDs in Table 8. The correctly fixed solutions are determined from a reference set of ambiguities. The reference ambiguities were estimated by using a dual-frequency four-system model, with fixed precise benchmark coordinates, making use of a 10° elevation cut-off angle and treating the ambiguities as time-constant over the entire observation time span.

Table 9: Empirical STDs for ionosphere-float, ZTD-float dual-frequency RTK and a cut-off angle of 10°, ambiguity float/correctly fixed solutions in North, East and Up. The L1,L2 QZSS-GPS code/phase ISBs are assumed fixed (and within brackets the ISBs-float case is given as well). The STDs are based on re-initializations of the Kalman filter during 9 hours in February 19, 2014 and when the bootstrapped SR criterion in (15) of 99.9% is fulfilled. In the last column the corresponding # of epochs needed is depicted as well.

System/frequency	Empirical STDs float/correctly fixed			# epochs
	N [cm]	E [cm]	U [cm]	[30 s]
L1,L2 GPS	7.3/0.9	21.4/0.9	21.6/3.3	41
L1,L2+E1,E5a+L1,L2	8.3/0.7	14.7/0.8	23.5/3.0	32
GPS+Galileo+QZSS	(8.1/0.8)	(17.7/0.8)	(20.7/3.6)	36
L1,L2+E1,E5a+L1,L2+B1,B2	7.2/0.6	11.0/0.6	15.5/2.9	28
GPS+Galileo+QZSS+BDS	(7.6/0.6)	(12.2/0.6)	(15.4/3.2)	29

The empirical STDs in Table 9 are in overall in good agreement with the formal precisions given in Table 8, with somewhat more optimistic formal STDs. Note however that the precision of e.g. the GPS+Galileo+QZSS ISBs-fixed ambiguity-float North and Up components now are slightly larger than for GPS. However this model also has a smaller TTFF of 32 epochs vs 41 epochs for GPS which explain these differences, since the ambiguity-float STDs improve with respect to time. Moreover when combining the systems we can thus reliably fix the ambiguities faster and allow for the precise mm-cm-level positioning at an earlier stage. This will be further elaborated on in the following two sections.

Positioning for higher elevation cut-off angles

When combining the systems higher than customary elevation cut-off angles can be allowed [8], which can be of particular benefit in urban canyon environments or when low elevation-multipath might be present. We depict a snapshot example in Figure 6 for the dual-frequency

ionosphere-float, ZTD-float horizontal (N,E) and vertical (U) RTK positioning and a cut-off angle of 20°, based on real data. The correctly fixed solutions are depicted as green, the wrongly fixed as red, and the float solutions as gray. Under each positioning model we also present the corresponding bootstrapped SR time-series and the total number of satellites as light green. As to illustrate two different convergence time periods the Kalman filter is re-initialized after 300 epochs (150 minutes). The number of Galileo (dark green), QZSS (cyan) and BDS (magenta) satellites is depicted as well.

Figure 6 illustrates that the time until the ambiguities can be fixed for the combined systems is much shorter in comparison to GPS. It is namely sufficient with 53 epochs as TTFF (using the criterion in (15)) at the first initialization for GPS+Galileo+QZSS (ISBs-fixed) to allow for precise ambiguity-fixed positioning availability, whereas for GPS 82 epochs are required. The improvement for this 3-system model is even more significant when all three Galileo satellites are visible, where the TTFF improve to 25 epochs for the second (re-)initialization in comparison to GPS that requires 75 epochs. When BDS is added the TTFFs are further improved, particularly in comparison to the first initialization of the other two models with a TTFF of 17 epochs.

In Figure 7 we give the correctly fixed formal STDs corresponding to the Up-components in Figure 6. Since we use an elevation-weighting strategy in our stochastic model, the formal STDs mostly depend on the satellite geometry and the number of satellites. This illustrates that the performance of ambiguity resolution and positioning do not always go hand-in-hand [8, 20]. For instance when looking into the largest GPS-only Up-component positioning errors in Figure 6 that corresponds to the period of largest formal STDs in Figure 7, we can still correctly fix our ambiguities because of the bootstrapped SRs larger than 99.9%. Fortunately however we have improvements both in formal STDs in Figure 7 and the Up-component positioning errors in Figure 6, particularly between $1 - 600$ epochs, when combining the systems with GPS. The best improvement can be seen when BDS is added to the systems. Note finally in Figure 6 that there are a few epochs where the solutions are incorrectly fixed (red) for the 4-system model at an early stage of the first initialization, due to a BDS satellite that rises at an elevation angle of 20° in combination with site-specific multipath effects. However as a few number of epochs passes the solutions become correctly fixed (green) as predicted by the bootstrapped SR.

On the ambiguity-float RTK positioning convergence time and the improvement by ambiguity-fixing

The purpose of integer ambiguity resolution is to improve the other parameters by the integer constrains, such as the receiver positions. However once the float ambiguities have converged to deterministic values, the ambiguity-float RTK positioning solutions can also start to take advantage of the very precise phase measurements and integer ambiguity resolution makes less sense. In other words, the faster we are allowed to do integer ambiguity resolution the more will the positions improve.

The ambiguity-float positioning convergence time criterion that we will use follows as,

$$\sqrt{|Q_{\hat{N}\hat{E}\hat{U}}|}^{\frac{1}{3}} \leq \sqrt{|Q_{\check{N}\check{E}\check{U}}|}^{\frac{1}{3}} + 0.01 \quad [\text{m}] \qquad (16)$$

where $Q_{\hat{N}\hat{E}\hat{U}}$ is the formal ambiguity-float position VCV-matrix, 3 is the dimension of the N, E and U positioning vector, and $Q_{\check{N}\check{E}\check{U}}$ is the formal ambiguity-fixed position VCV-matrix. Compare this expression to the ADOP in (14). As the determinant is used, the covariances between the coordinate components are taken into account as well. When the ambiguity-float geometric average on the left hand side of (16) is 1 cm from the ambiguity-fixed geometric average on the right, we can determine the convergence time. Thus we consider here the float and fixed solution of similar quality if they differ less than 1 cm.

We depict the ambiguity-float (gray) and ambiguity-fixed (magenta) geometric averages (16) in Figure 8 corresponding to the positioning results for the 20° cut-off angle in Figure 6. The ambiguity-fixed geometric averages start at the same time-instances as the bootstrapped SR reaches 99.9% in Figure 6, and these times are depicted by vertical dotted blue lines. The ambiguity-float positioning convergence times as determined by (16) are depicted by vertical dashed black lines and at bottom of each RTK model we give the ADOPs as well. Note that the Kalman filter is re-initialized after 300 epochs.

Figure 8 shows that the GPS-only (top) ionosphere-float model in this case has up to 83 minutes of ambiguity-float positioning convergence time (second (re-)initialization). The corresponding time for the GPS+Galileo+QZSS model (middle) is 45.5 minutes, and 32 minutes for the 4-systems (bottom). Moreover the ADOPs are below the 0.12 cycle level once the ambiguity-fixed positioning precisions become available for each model. Most importantly we can conclude from Figure 8 that GPS-only ionosphere-float RTK positioning cannot benefit as significantly from fast reliable integer ambiguity resolution as the corresponding three and 4-system models. This since we have an ambiguity-float geometric average at the level of 5 cm for GPS-only once the bootstrapped SR is 99.9%, whereas the combined 3-
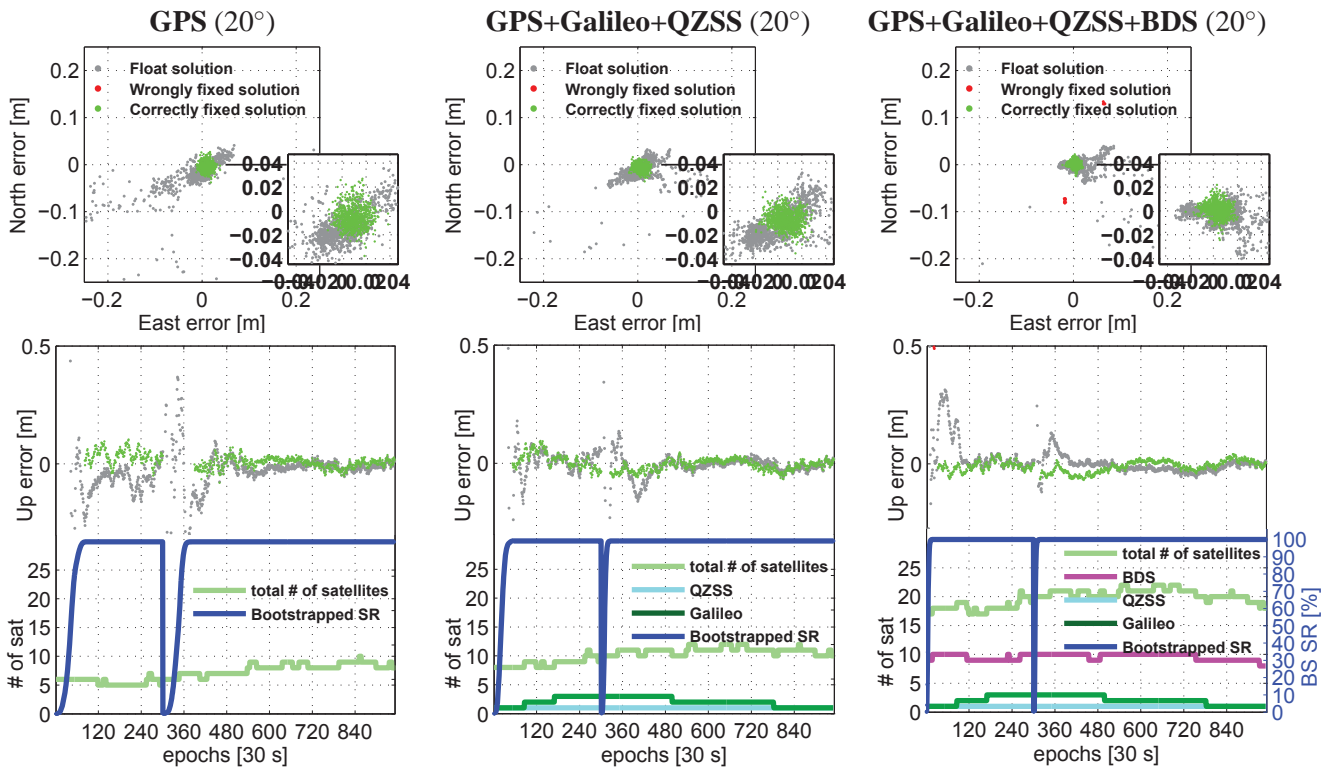
Figure 6: *Top* ionosphere-float, ZTD-float L1,L2 GPS (*left*), ISBs-fixed L1,L2+E1,E5a+L1,L2 GPS+Galileo+QZSS (*middle*) and ISBs-fixed L1,L2+E1,E5a+L1,L2+B1,B2 GPS+Galileo+QZSS+BDS (*right*) RTK for a 20° cut-off angle. At *bottom* the total # of satellites is depicted as *light green* and the bootstrapped SR time-series in *blue*. The Kalman filter is re-initialized after 300 epochs. The # of epochs to reach bootstrapped SR in (15) of 99.9% (2:nd initialization in brackets): 41 (37.5) min for GPS (*left*), 26.5 (12.5) min for GPS+Galileo+QZSS (*middle*), and 8.5 (8) min for GPS+Galileo+QZSS+BDS (*right*)

| (a) GPS | (b) GPS+Galileo+QZSS | (c) GPS+Galileo+QZSS+BDS |
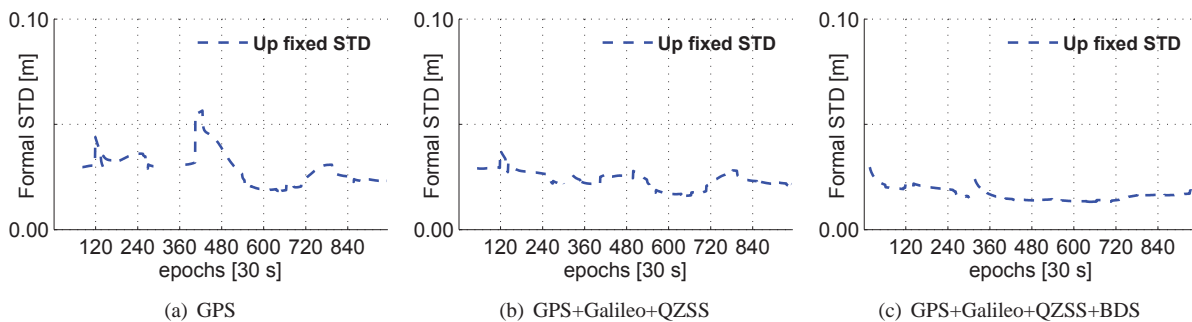
Figure 7: Dual-frequency ionosphere-float, ZTD-float Up correctly fixed formal STDs corresponding to Figure 6, cut-off angle of 20°

systems have a value close to 10 cm (for the second (re-) initialization), and the 4-system model values even up to 15 cm. Thus we can conclude from Figure 8 that when using an elevation cut-off angle of 20° the combination of the four systems can provide for faster reliable ambiguity-fixed positioning precisions, shorter ambiguity-float positioning convergence times, and give larger precision improvements when going from ambiguity-float to ambiguity-fixed positioning, all in comparison to GPS and the 3-system model.

CONCLUSIONS

In this contribution we studied the combination of dual-frequency L1,L2 GPS, E1,E5a Galileo, L1,L2 QZSS and B1,B2 BDS for long single-baseline RTK. With long

baseline we refer to the necessity to model the slant ionospheric delays by the ionosphere-float strategy as well as the residual (wet) Zenith Tropospheric Delay (ZTD). The code/phase inter-system biases (ISBs) were moreover fixed when possible to maximize the redundancy of the models, which also allows for a common pivot satellite between the systems. The analysis was based on real GNSS data collected in Perth, Australia. We can summarize our main findings and conclusions as follows.
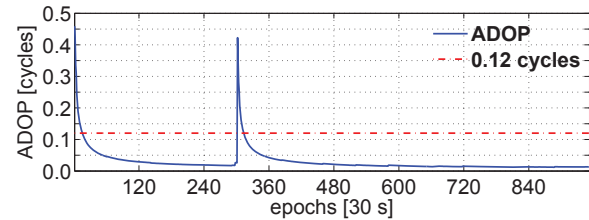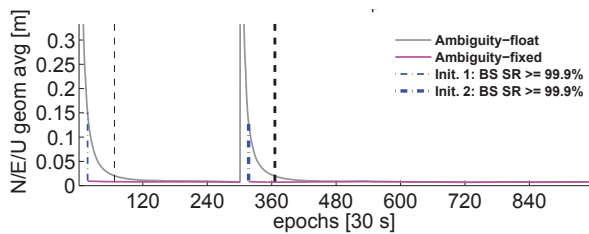
Inter-system biases

We illustrated that at least two overlapping frequencies are needed for calibration of ISBs to increase the redundancy for the ionosphere-float model and in comparison to when the ISBs are estimated. This since the code ISBs
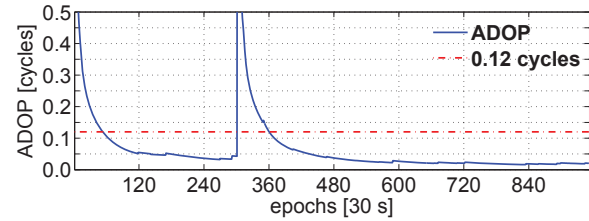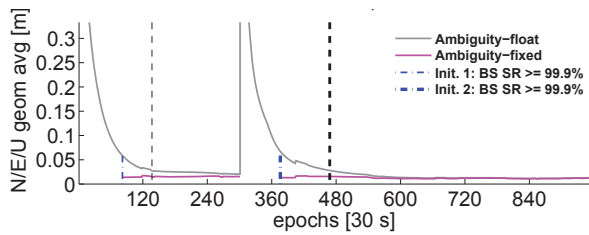
(a) L1,L2 GPS
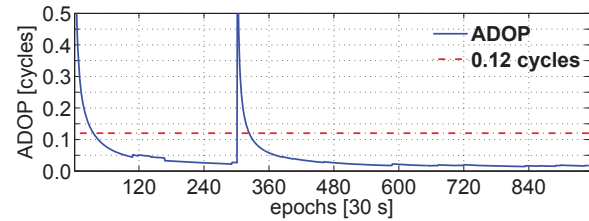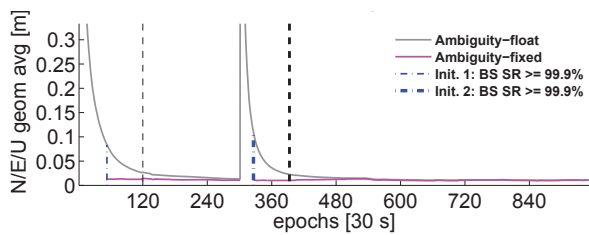
(b) ISBs-fixed: L1,L2+E1,E5a+L1,L2 GPS+Galileo+QZSS

(c) ISBs-fixed: L1,L2+E1,E5a+L1,L2+B1,B2 GPS+Galileo+QZSS+BDS

Figure 8: Ambiguity-float positioning convergence time for a 20° cut-off angle, where the dual-frequency ionosphere-float, ZTD-float and ambiguity-float (gray) and ambiguity-fixed (magenta) geometric averages (16) are given, and at bottom the corresponding ADOP time-series. The convergence times are given as (2:nd initialization in brackets): 68.5 (83) min for GPS, 60 (45.5) min for GPS+Galileo+QZSS, and 33.5 (32) min for GPS+Galileo+QZSS+BDS

are only estimable on the second frequency and beyond. The code/phase ISBs of L1,L2 QZSS-GPS were safely neglected throughout this study as similar Trimble NetR9 receiver types were used [15].

Instantaneous RTK and time to first fix

As to investigate whether instantaneous RTK is possible for the ionosphere-float model, a formal ambiguity dilution of precision (ADOP) analysis was conducted. It was predicted that successful instantaneous single-baseline RTK is not possible, and a Kalman filter with a dynamic model is thus needed. The time to first fix (TTFF) was computed for the different combinations of the four systems, as the accumulated time necessary in the Kalman filter to reach an integer bootstrapped success rate of 99.9%. The combination of Galileo and QZSS with GPS provided for smaller TTFFs in comparison to using GPS separately. The improvements were more significant when the code/phase ISBs were fixed and/or when BDS was added to the three systems. The conclusion is therefore that calibration of ISBs is particularly important in environments with obstructed satellite visibility, as each satellite added to GPS can then contribute to the solution as if it was an additional satellite from the same system.

Ambiguity-float vs ambiguity-fixed positioning precisions

The empirical positioning precisions as determined by comparing the estimated positions to precise benchmark coordinates were shown to be in overall good agreement with the formal precisions, with the somewhat more optimistic formal precisions. Most importantly it was shown that the combined systems allow for faster ambiguity-float positioning precisions at the dm-level, shorter TTFFs and thus faster availability of ambiguity-fixed position precisions at the mm-cm level. This was particularly true when all four systems were combined and the code/phase ISBs were fixed. When looking into the positioning results for an elevation cut-off angle of 20°, it could moreover be concluded that the combined systems provide for improved receiver-satellite geometry and thus more precise positioning in comparison to GPS-only RTK.

Position-precision improvement by ambiguity-fixing

The faster we can reliably fix the ambiguities the more will the integer constrains improve the receiver positions. It was found for the elevation cut-off angle of 20° that the 4-system model allows for larger precision improvements when going from ambiguity-float to ambiguity-fixed RTK positioning, and as compared to the GPS and GPS+Galileo+QZSS models.

ACKNOWLEDGEMENTS

REFERENCES

[1] Mirgorodskaya, T., "GLONASS government policy, status and modernization plans," in *Proceedings of international global navigation satellite systems (IGNSS) symposium*, (Golden Coast), 16-18 July, 2013.

[2] CSNO, "BeiDou Navigation Satellite System Signal In Space Interface Control Document by China Satellite Navigation Office (CSNO). Open service signal B1I (Version 1.0)," tech. rep., December 2012. 77 pages., 2012.

[3] ESA, "Galileo In-Orbit Validation," in *Fact sheet by European space agency (ESA)*, 2013.

[4] J. Boyd, "Japans Plan for Centimeter-Resolution GPS," in *IEEE Spectrum, news*, 23 April 2014.

[5] C. Shi, Q. Zhao, Z. Hu, and J. Liu, "Precise relative positioning using real tracking data from COMPASS GEO and IGSO satellites," *GPS Solutions*, vol. 17, no. 1, pp. 103–119, 2013. doi:10.1007/s10291-012-0264-x.

[6] O. Montenbruck, A. Hauschild, P. Steigenberger, U. Hugentobler, P. J. G. Teunissen, and S. Nakamura, "Initial assessment of the COMPASS/BeiDou-2 regional navigation satellite system," *GPS Solutions*, vol. 17, no. 2, pp. 211–222, 2013.

[7] R. Odolinski, P. J. G. Teunissen, and D. Odijk, "Quality analysis of a combined COMPASS/BeiDou-2 and GPS RTK positioning model," in *International Global Navigation Satellite Systems Society IGNSS symposium*, (Golden Coast), 16-18 July 2013.

[8] P. J. G. Teunissen, R. Odolinski, and D. Odijk, "Instantaneous BeiDou+GPS RTK positioning with high cut-off elevation angles," *J. Geodesy*, vol. 88, no. 4, pp. 335–350, 2014. doi:10.1007/s00190-013-0686-4.

[9] Y. Yang, J. Li, A. Wang, J. Xu, H. He, H. Guo, J. Shen, and X. Dai, "Preliminary assessment of the navigation and positioning performance of BeiDou regional navigation satellite system," *Science China, Earth Sciences*, vol. 57, no. 1, pp. 144–152, 2014.

[10] N. Nadarajah, P. J. G. Teunissen, J.-M. Sleewaegen, and O. Montenbruck, "The mixed-receiver BeiDou inter-satellite-type bias and its impact on RTK positioning," *GPS Solutions*, 2014. doi:10.1007/s10291-014-0392-6.

[11] D. Odijk and P. J. G. Teunissen, "Characterization of between-receiver GPS-Galileo inter-system biases and their effect on mixed ambiguity resolution," *GPS Solutions*, vol. 17, no. 4, pp. 521–533, 2013.

[12] O. Montenbruck, A. Hauschild, and U. Hessels, "Characterization of GPS/GIOVE sensor stations in the CONGO network," *GPS Solutions*, vol. 15, no. 3, pp. 193–205, 2011.

[13] T. Melgard, J. Tegedor, K. de Jong, D. Lapucha, and G. Lachapelle, "Interchangeable integration of GPS and Galileo by using a common system clock in PPP," in *Proceedings of ION GNSS*, (Nashville, TN), pp. 1198–1206, 16–20 September 2013.

[14] D. Odijk and P. J. G. Teunissen, "Estimation of differential inter-system biases between the overlapping frequencies of GPS, Galileo, BeiDou and QZSS," in *4th International Colloquium Scientific and Fundamental Aspects of the Galileo Programme*, (Prague, Czech Republic), 4–6 December 2013.

[15] R. Odolinski, P. J. G. Teunissen, and D. Odijk, "Combined BDS, Galileo, QZSS and GPS single-frequency RTK," *GPS Solutions*, 2014. doi:10.1007/s10291-014-0376-6.

[16] P. J. G. Teunissen, "Generalized inverses, adjustment, the datum problem and S-transformations," *In: Grafarend EW, Sanso F (eds) Optimization of geodetic networks*, 1985. Springer, Berlin, pp 11-55.

[17] P. J. G. Teunissen, D. Odijk, and B. Zhang, "PPP-RTK: Results of CORS network-based PPP with integer ambiguity resolution," *J Aeronaut, Astronaut and Aviat, Ser A*, vol. 42, no. 4, pp. 223–230, 2010.

[18] J. Saastamoinen, "Contributions to the theory of atmospheric refraction," *Bull Geod*, vol. 105, no. 1, pp. 279–298, 1972.

[19] C. R. Rao, *Linear statistical inference and its applications, 2nd edition*. Wiley, New York, 1973.

[20] P. J. G. Teunissen, "A canonical theory for short GPS baselines. Part I: The baseline precision, Part II: The ambiguity precision and correlation, Part III: The geometry of the ambiguity search space, Part IV: Precision versus reliability," *J. Geodesy*, vol. 71(6):320-336, 71(7):389-401, 71(8):486-501, 71(9):513-525, 1997.

[21] H. J. Euler and C. G. Goad, "On optimal filtering of GPS dual frequency observations without using orbit information," *Bull Geod*, vol. 65, pp. 130–143, 1991.

[22] P. J. G. Teunissen, "An integrity and quality control procedure for use in multi sensor integration," in *Proc of ION GPS*, (CO), pp. 513–522, September 1990. Also in: Vol VII of GPS Red Book Ser: Integr syst, ION Navig, 2012.

[23] P. J. G. Teunissen, "The least squares ambiguity decorrelation adjustment: a method for fast GPS integer estimation," *J. Geodesy*, vol. 70, pp. 65–82, 1995.

[24] Schüler, T., "On ground-based GPS tropospheric delay estimation," *Ph.D. dissertation, Universität der Bundeswehr, Munich, Germany*, 2001. 364 pages.

[25] P. J. G. Teunissen, P. de Jonge, and C. Tiberius, "The volume of the GPS ambiguity search space and its relevance for integer ambiguity resolution," in *"Proc ION GPS*, vol. 9, pp. 889–898, 1996.

[26] D. Odijk and P. Teunissen, "ADOP in closed form for a hierarchy of multi-frequency single-baseline GNSS models," *J. Geodesy*, vol. 82, pp. 473–492, 2008.

[27] R. Odolinski, P. J. G. Teunissen, and D. Odijk, "An analysis of combined COMPASS/BeiDou-2 and GPS single- and multiple-frequency RTK positioning.," in *ION Pacific PNT, Honolulu, HI, USA*, pp. 69–90, 2013.

[28] B. Schaffrin and Y. Bock, "A unified scheme for processing GPS dual-band phase observations," *Bull Geod 62*, pp. 142–160, 1988.

[29] P. J. G. Teunissen, "Success probability of integer GPS ambiguity rounding and bootstrapping.," *J. Geodesy*, vol. 72, pp. 606–612, 1998.

[30] P. J. G. Teunissen, "An optimality property of the integer least-squares estimator.," *J. Geodesy*, vol. 73, pp. 587–593, 1999.

[31] W. Melbourne, "The case for ranging in GPS-based geodetic systems," in *Proceedings of 1st International Symposium on Precise Positioning with the Global Positioning System*, (Rockville, MD, USA), pp. 373–386, 1985.

[32] G. Blewitt, "Carrier phase ambiguity resolution for the global positioning system applied to geodetic baselines up to 2000 km," *J Geophys Res 94(B8)*, pp. 10187–10203, 1989.

[33] G. Wang, K. d. Jong, Q. Zhao, Z. Hu, and J. Guo, "Multipath analysis of code measurements for BeiDou geostationary satellites," *GPS Solutions*, 2014. doi:10.1007/s10291-014-0374-8.

A DESCRIPTION OF THE ISBS-FLOAT RANK DEFICIENCIES

For the derivations in Table 2 we have assumed the baseline length to be of less than a few hundred kilometers, consequently giving line-of-sight unit vectors and mapping functions for the Zenith Tropospheric Delay (ZTD) that are similar between the receivers. This makes rise to 4 rank deficiencies that are solved by fixing the pivot receiver 1 coordinates (x_1) and ZTD (τ_1). This follows by 1 rank defect between the columns of the receiver clocks that is eliminated by fixing the pivot receiver 1 clock (dt_1), and 1 rank defect between the columns of the receiver 2 clock and GPS hardware (HW) code/phase

delays that is solved by fixing the GPS HW code delay on the first frequency for receiver 2 $\left(d_{2,1}^G\right)$. Then we have 1 rank defect between the columns of the receiver clock, HW code/phase delays/ISBs and GPS ionospheric delays, which is solved by fixing the GPS HW code delay on the second frequency for receiver 2 $\left(d_{2,2}^G\right)$. The $m_G + m_*$ rank defects between the columns of the slant ionospheric delays are solved by fixing the pivot receiver 1 corresponding delays $\left(\iota_1^{s_G}, \iota_1^{s_*}\right)$.

Then there are $3 \cdot 1$ (3 corresponds to three additional systems to GPS) rank defects between the HW code/phase delays/ISBs and ionosphere of system $*$, which are solved by fixing the HW code delay on the first frequency for the second receiver for that system $\left(d_{2,1}^*\right)$. Following that the rank deficiencies between columns of the HW code/phase delays/ISBs of size $2f + 3 \cdot 2f$ are solved by fixing pivot receiver 1 HW code/phase delays on all frequencies for all systems $\left(d_{1,j}^G, \delta_{1,j}^G, d_{1,j}^*, \delta_{1,j}^*\right)$. Then we have the rank deficiency of size $f + 3 \cdot f$ between the columns of the HW phase delays/ISBs and ambiguities, which are solved by fixing the ambiguities on all frequencies for receiver 2 and the pivot satellite 1 for all systems $\left(z_{2,j}^{1_G}, z_{2,j}^{1_*}\right)$. Finally we have a rank deficiency of size $fm_G + fm_*$ between the columns of the ambiguities that are solved by fixing the ambiguities on all frequencies, for all satellites, the pivot receiver 1 and all systems $\left(z_{1,j}^{s_G}, z_{1,j}^{s_*}\right)$.